A benchmark for non-covalent interactions in solids

A. Otero-de-la-Roza and Erin R. Johnson

Citation: J. Chem. Phys. **137**, 054103 (2012); doi: 10.1063/1.4738961
View online: http://dx.doi.org/10.1063/1.4738961
View Table of Contents: http://jcp.aip.org/resource/1/JCPSA6/v137/i5
Published by the American Institute of Physics.

A benchmark for non-covalent interactions in solids

A. Otero-de-la-Roza[a] and Erin R. Johnson[b]
Chemistry and Chemical Biology, School of Natural Sciences, University of California, Merced, 5200 North Lake Road, Merced, California 95343, USA

(Received 29 May 2012; accepted 10 July 2012; published online 1 August 2012)

A benchmark for non-covalent interactions in solids (C21) based on the experimental sublimation enthalpies and geometries of 21 molecular crystals is presented. Thermal and zero-point effects are carefully accounted for and reference lattice energies and thermal pressures are provided, which allow dispersion-corrected density functionals to be assessed in a straightforward way. Other thermal corrections to the sublimation enthalpy (the 2*RT* term) are reexamined. We compare the recently implemented exchange-hole dipole moment (XDM) model with other approaches in the literature to find that XDM roughly doubles the accuracy of DFT-D2 and non-local functionals in computed lattice energies (4.8 kJ/mol mean absolute error) while, at the same time, predicting cell geometries within less than 2% of the experimental result on average. The XDM model of dispersion interactions is confirmed as a very promising approach in solid-state applications. © *2012 American Institute of Physics*. [http://dx.doi.org/10.1063/1.4738961]

I. INTRODUCTION

Dispersion interactions[1–4] are essential in a collection of active research fields in solid-state physics and chemistry, including molecular crystal packing,[5,6] crystal structure prediction,[7] surface adsorption and reactivity,[2] and supramolecular chemistry.[8] The representation of dispersion interactions in density-functional theory (DFT) is not possible within local or semilocal functionals because dispersion arises from non-local correlation effects involving distant fragments in the crystal.[1] In recent years, the dispersion problem has been one of the primary fronts of research in DFT,[9] and new ideas to incorporate dispersion effects into the otherwise excellent semilocal description of hard matter are being proposed regularly to this day.[10] Because of the paramount importance DFT has among solid-state electronic structure methods, a set of reference data to assess the performance of new functionals for non-covalent interactions would be very useful.

In sharp contrast with the abundance of good-quality reference datasets in molecular quantum chemistry,[11–16] these are rare in the solid-state. The usual procedure to assess the performance of dispersion-corrected density functionals is to examine a restricted number of very well studied weakly bound crystals[17–31] or to reproduce gas-phase results using the datasets mentioned above.[17,32,33] There are two reasons for this lack of reference data: (i) accurate wavefunction calculations are very difficult to apply to solids except case-by-case (for instance, Refs. 34 and 19), and (ii) experimental data needs careful correction for thermal and zero-point effects in order to compare to static DFT results. In the case of lattice energies, this correction introduces an uncertainty that, combined with experimental errors, limits the insight to be gained from the comparison.[35]

One of the objectives of this work is to present good-quality reference data derived from experimental results on molecular crystals (the C21 set) to allow the straightforward testing of new density functionals. Such benchmark sets exist in the case of hard solids (see Ref. 36 and references therein) and compilations of experimental binding energies of molecular crystals are available[6,22,35] that use a simple correction to reduce thermal effects (the 2*RT* term). However, as we shall see below, this procedure has its limitations and, to our knowledge, there are no test sets in the literature that include a proper thermal and zero-point effect correction to binding energies or that provide reference data for crystal geometries.

The crystal equivalent of the binding energy of a dimer, the lattice energy, is related to the experimental sublimation enthalpy of a molecular crystal, for which an extensive database is available.[37] Regarding geometries, diffraction experiments provide very accurate cell lengths and atomic positions of a periodic crystal at a given temperature. Thermal effects on both sublimation enthalpies and crystal geometries are accounted for in this article using a combination of accurate DFT vibrational frequencies and numerical and physical approximations. The soundness of these approximations is checked against a simple molecular crystal (carbon dioxide) and is confirmed *a posteriori* by the excellent results some of the dispersion-corrected functionals offer. The proposed reference values, if not as accurate as their molecular counterparts, provide a stepping-stone for dispersion-related density functional development in solids.

The second objective in this work is to assess the performance of the exchange-hole dipole moment (XDM) model,[13,14,30,38–46] recently implemented for solids,[30] compared to other dispersion functionals in the literature. The choice of functionals has been guided by availability, popularity, and computational simplicity: in addition to XDM, we have chosen the DFT-D2 method by Grimme,[47] the Tkatchenko-Scheffler scheme,[32] and two non-local functionals by Langreth *et al.*[33,48] As pointed out by Tkatchenko

[a]Electronic mail: aoterodelaroza@ucmerced.edu.
[b]Electronic mail: ejohnson29@ucmerced.edu.

et al.,[2] the accuracy of these methods has not been fully established in solids. As we show below, the excellent performance of the XDM model opens new exciting perspectives in the first-principles prediction of surface adsorption energies, polymorph ranking, molecular crystal phase transitions, and *ab initio* molecular dynamics.

II. DISPERSION MODELS

In this section, we review the dispersion models we compare using our C21 test set. The choice of methods has been guided by three criteria: (i) availability, (ii) popularity in condensed-matter studies, and (iii) modest computational cost. In the following, we give a brief description of the XDM model on account of its novelty in solid-state studies.

The XDM model, developed by Becke and Johnson[13,14,30,38–46] describes the dispersion energy of two neutral fragments as the electrostatic interaction of the dipoles formed by electrons and their associated exchange holes. The dispersion energy is added to the DFT energy

$$E = E_{\mathrm{DFT}} + E_{\mathrm{disp}}, \tag{1}$$

where the E_{disp} contains the usual R^{-6} leading term as well as two additional higher order atomic-pairwise terms

$$E_{\mathrm{disp}} = -\frac{1}{2}\sum_{ij}\sum_{n=6,8,10}\frac{C_{n,ij}}{R^n_{\mathrm{vdw},ij} + R^n_{ij}}. \tag{2}$$

The fundamental objects in this equation are the interatomic interaction coefficients $C_{n,ij}$ that in the XDM model are calculated exclusively from first-principles quantities using second-order perturbation theory[44]

$$C_{6,ij} = \frac{\alpha_i\alpha_j\left\langle M_1^2\right\rangle_i\left\langle M_1^2\right\rangle_j}{\left\langle M_1^2\right\rangle_i\alpha_j + \left\langle M_1^2\right\rangle_j\alpha_i}, \tag{3}$$

$$C_{8,ij} = \frac{3}{2}\frac{\alpha_i\alpha_j\left(\left\langle M_1^2\right\rangle_i\left\langle M_2^2\right\rangle_j + \left\langle M_2^2\right\rangle_i\left\langle M_1^2\right\rangle_j\right)}{\left\langle M_1^2\right\rangle_i\alpha_j + \left\langle M_1^2\right\rangle_j\alpha_i} \tag{4}$$

$$C_{10,ij} = 2\frac{\alpha_i\alpha_j\left(\left\langle M_1^2\right\rangle_i\left\langle M_3^2\right\rangle_j + \left\langle M_3^2\right\rangle_i\left\langle M_1^2\right\rangle_j\right)}{\left\langle M_1^2\right\rangle_i\alpha_j + \left\langle M_1^2\right\rangle_j\alpha_i} + \frac{21}{5}\frac{\alpha_i\alpha_j\left\langle M_2^2\right\rangle_i\left\langle M_2^2\right\rangle_j}{\left\langle M_1^2\right\rangle_i\alpha_j + \left\langle M_1^2\right\rangle_j\alpha_i}, \tag{5}$$

where α_i are the atomic polarizabilities and $\langle M_l^2\rangle_i$ are the expectation values of the square of the atomic l-moments. In order to define atomic quantities, the Hirshfeld partitioning scheme[49] is used.[13] For instance, atom-in-molecule polarizabilities are obtained by scaling the free-atom values (α_{free}) with Hirshfeld volumes[50]

$$\alpha_i = \frac{\int r^3\omega_i(\mathbf{r})\rho(\mathbf{r})d\mathbf{r}}{\int r^3\rho_{i,\mathrm{free}}(\mathbf{r})d\mathbf{r}}\alpha_{i,\mathrm{free}}, \tag{6}$$

where $\omega_i(\boldsymbol{r})$ is the Hirshfeld weight, ρ is the electron density and $\rho_{i,\mathrm{free}}$ is the free-atom electron density. In a similar vein, the moments are computed as:

$$\left\langle M_l^2\right\rangle_i = \sum_\sigma\int\omega_i(\mathbf{r})\rho_\sigma(\mathbf{r})\left[r_i^l - (r_i - d_{X\sigma})^l\right]^2 d\mathbf{r} \tag{7}$$

where ρ_σ is the spin density, r_i is the distance from nucleus i, and $d_{X\sigma}$ is the magnitude of the exchange-hole dipole moment.

The exchange-hole dipole moment is the fundamental quantity in the XDM dispersion model (hence its name) and can be computed in two ways. In the original version,[39] the exact exchange-hole is used, an approach that is computationally demanding, particularly using a plane-wave basis-set. To avoid this, the Becke-Roussel (BR) (Ref. 51) model of the exchange hole is used in its place.[14,40,45] The BR model depends exclusively on local quantities ($\rho, \nabla^2\rho, \tau$) so the XDM-corrected functional (Eq. (1)) formally represents a meta-generalized gradient approximation (meta-GGA) functional. Indeed, the derivation of the potential and the self-consistent implementation of XDM has been reported before[52] and the authors show that there is little difference between the self-consistent and the post-SCF approaches. As a consequence, we use the post-SCF XDM dispersion, purely for practical reasons. Also, it should be noticed that the calculation of the dispersion correction adds negligibly to the total computational cost.

All the equations above are parameter-free, except for the damping expression in Eq. (2). The interatomic van der Waals radii ($R_{\mathrm{vdw},ij}$) control the distance at which the pairwise dispersion interactions are switched off, and are defined using two parameters, a_1 and a_2,

$$R_{\mathrm{vdw},ij} = a_1 R_{c,ij} + a_2, \tag{8}$$

$$R_{c,ij} = \frac{1}{3}\left[\left(\frac{C_{8,ij}}{C_{6,ij}}\right)^{1/2} + \left(\frac{C_{10,ij}}{C_{6,ij}}\right)^{1/4} + \left(\frac{C_{10,ij}}{C_{8,ij}}\right)^{1/2}\right], \tag{9}$$

where $R_{c,ij}$ are the critical radii. The value of these parameters has been obtained by fitting to a training set both in gas-phase[14,45] and under periodic-boundary conditions.[30] In the last case, the training set consisted of binding energies of dimers and not crystals, as would have been reasonable, precisely because of the mentioned lack of proper solid-state training sets.

Because the dispersion coefficients are calculated rather than fitted, Eq. (1) works under the assumption that the DFT functional presents a completely dispersionless behavior. This requirement is not met by most GGA functionals, which are sometimes too repulsive and sometimes spuriously binding, depending on the reduced-density-gradient tail behavior of the exchange enhancement factors.[45,53] In previous articles,[45,53] it has been shown that the Becke86 (Ref. 54) (B86b) and Perdew-Wang86 (Ref. 55) (PW86) exchange functionals best describe the Hartree-Fock-like repulsive wall. When coupled with any other exchange functional (for instance, Perdew-Burke-Ernzerhof, PBE; Ref. 56), the parameters in Eq. (2) account partially for the erroneous behavior of the exchange energy. As a consequence, B86b and PW86 perform systematically better than the other functionals studied

as shown in previous studies[14,30] and below. In this work, we use two XDM-corrected functionals: (i) B86b exchange with PBE correlation (B86b-XDM), and (ii) PBE (PBE-XDM).

In addition to XDM, we consider several popular dispersion models in the literature. The simplest and most widespread approach, both in molecular and solid-state calculations, is the DFT-D method, popularized by Grimme.[23,47,57] As in the case of XDM, the DFT-D method is based on the calculation of $E_{\rm disp}$ (Eq. (1)) using an attenuated dispersion formula. The like-atom interaction coefficients $C_{6,ii}$ as well as the van der Waals radii are tabulated using a combination of computed and experimental data. The unlike-atom coefficients are calculated using a geometric-mean combination formula. This approach is sometimes coupled with the modification of the parameters in the non-dispersion part of the density functional (the B97D functional[47]).

The DFT-D2 functional[47] presents some drawbacks: (i) the expansion of the dispersion energy is truncated at the R^{-6} term, while it is known that higher order terms may be important for its accurate description,[13,30] (ii) the interaction coefficients do not respond to changes in the chemical environment,[58] and (iii) while the main-group elements are reasonably well represented, the interaction coefficients for transition metals are rather poor (all first-row transition metals are represented by the same $C_{6,ii}$, for instance). In spite of these problems, the statistics of DFT-D2 when applied to S22 are good[59] (for instance, a mean absolute error of 0.44 kcal/mol using B97D), especially taking into account the simplicity of the model. It has also been parametrized for a large number of functionals and extensively tested.[60] Because forces and stresses are easily calculated,[23] DFT-D2 is present in most quantum chemistry and solid-state codes and provides a cheap way to avoid the appalling deficiency of common GGAs for dispersion-bound crystals, explaining its popularity. A newer version of DFT-D (DFT-D3) has been recently proposed[60] that tries to correct the problems mentioned above, but it is not as fully established or widely available as its older relative. In this work, we will use DFT-D2 combined with the PBE functional, as implemented in Quantum ESPRESSO by Barone *et al.*[23] (PBE-D).

The method by Tkatchenko and Scheffler[32] (TS) also calculates the asymptotic dispersion energy in Eq. (1). Similar to DFT-D, the dispersion expansion is truncated at the leading-order R^{-6} term. The interaction coefficients are calculated from the like-atom values using an expression derived from the London formula. The characteristic point of deviation from DFT-D2, however, is that the homoatomic C_6 are calculated by scaling the free-atom values using Hirshfeld atomic volumes, therefore factoring in the effect of the chemical environment

$$C_{6,ii}^{\rm eff} = \left(\frac{V_i^{\rm eff}}{V_i^{\rm free}}\right)^2 C_{6,ii}^{\rm free}, \tag{10}$$

where $V_i^{\rm eff}$ is the atom-in-molecule Hirshfeld volume and $V_i^{\rm free}$ is the volume of the free atom. The free-atom $C_{6,ii}^{\rm free}$ coefficients are obtained from a database of reference values and the agreement of the calculated molecular C_6 with experimental coefficients is remarkable.[32] Thanks to the possibility of treating dispersion in different chemical environments, including metallic surfaces, the TS correction has been extensively used to study surface adsorption problems.[2] In this work, we apply it coupled with the PBE functional (PBE-TS).

Calculating the dispersion energy as in Eq. (2) presents drawbacks: (i) it is only valid at the infinite separation limit so a damping function is always required, which introduces some degree of parametrization, and (ii) the R^{-6} behavior is not always correct, for instance in the case of interacting conducting slabs.[4] Much work has been put into the design of *seamless* functionals that include a non-empirical non-local contribution and are able to treat covalent and non-covalent interactions on the same level. A well-known collection of non-local functionals has been proposed by Langreth and coworkers[33,48,61] and they are collectively referred to as vdw-DF. The functionals are based on the seminal work by Andersson *et al.*[62] and write the exchange-correlation energy as

$$E_{xc} = E_x^{\rm GGA} + E_c^{\rm LDA} + E_c^{nl}, \tag{11}$$

where they combine a GGA exchange functional, local density approximation (LDA) correlation and the non-local term that accounts for dispersion. The latter can be written in the most general form as double density integral of a non-local kernel $\phi(\boldsymbol{r}, \boldsymbol{r}')$,

$$E_c^{nl} = \frac{1}{2}\int d\boldsymbol{r} \int d\boldsymbol{r}' n(\boldsymbol{r})\phi(\boldsymbol{r}, \boldsymbol{r}')n(\boldsymbol{r}') \tag{12}$$

that is calculated using the density and its gradient at $\boldsymbol{r}$ and $\boldsymbol{r}'$.

Two well-studied versions of vdw-DF in the literature are the ones proposed by Dion *et al.*[48] (vdw-DF1), that was turned into a full-fledged self-consistent approach by Thonhauser *et al.*[61] and the more recent version of Lee *et al.*[33] (vdw-DF2). Contrary to the original Andersson-Langreth-Lundqvist functional, no *a priori* specification of the interacting fragments is required. The non-local correlation kernel is obtained by making successive approximations to the adiabatic connection fluctuation-dissipation formula[4] and the functional is seamless because E_c^{nl} vanishes in the uniform-gas limit, therefore recovering the (correct) LDA correlation. It would appear that the double integral in Eq. (12) is computationally expensive, but the cost of vdw-DF is actually only slightly higher than semilocal functionals.[63] The exchange functional is one of the major components modified from vdw-DF1 to vdw-DF2, again because a dispersionless exchange is required. The vdw-DF1 version uses the revised PBE exchange functional[64] (revPBE), while vdw-DF2 uses a revised PW86 functional[33] (rPW86). It has been shown[33] that this change improves the description of energetics and particularly geometries of solids, and we confirm below that this is indeed the case for molecular crystals as well.

III. COMPUTATIONAL DETAILS

The calculations have been carried out using a modified copy of Quantum ESPRESSO,[65] in which we have implemented the XDM method.[30] We have also incorporated the TS scheme as a simple offspring of the XDM code. In addition, DFT-D2 and both vdw-DF were already available, as implemented by other authors.[23,65] The vdw-DF functionals include the computation of forces and stresses, which

TABLE I. The column labels are, in order: the average over experimental sublimation enthalpy measurements corrected to room temperature (via C_p calculated by group additivity[37]), the relaxation energies (Eq. (15)), the deviation of the intermolecular vibrational contribution of the solid from the Dulong-Petit value ($6RT$), the intermolecular zero-point vibrational contribution of the solid, the difference between our correction to the lattice energy ($\Delta E_{\rm vib} + 4RT$ in Eq. (14)) and $-2RT$ (Eq. (17)), and the total thermal correction on sublimation enthalpies ($E_{\rm vib}^{\rm corr} = \Delta E_{\rm el}^{\rm exp} - \Delta H_{\rm sub}(T^0)$, $T^0 = 298.15$ K) . The last two columns are the reference data for the benchmark: experimental lattice energies and thermal pressures. Units are kJ/mol (energies) and GPa (pressures).

Name	$\Delta H_{\rm sub}^{\rm exp}(T^0)$	$\Delta E_{\rm vib}^{\rm relax}$	$\Delta E_{\rm vib}^{s,\rm inter}$	$E_{\rm vib,zp}^{s,\rm inter}$	$E_{\rm vib}^{\rm error}$	$E_{\rm vib}^{\rm corr}$	$\Delta E_{\rm el}^{\rm exp}$	$p_{\rm th}$
14-cyclohexanedione	81.13	−0.26	−2.08	2.25	0.42	5.40	86.53	0.275
Acetic acid	67.95	0.91	−2.85	3.29	−0.47	3.85	71.80	0.201
Adamantane	58.43	0.90	−1.63	1.74	−0.79	4.00	62.43	0.343
Ammonia	29.81	1.57	−5.87	10.72	3.28	7.76	37.57	0.592
Anthracene	98.17	2.06	−1.78	1.89	−1.95	2.40	100.58	0.224
Benzene	45.11	−0.12	−2.39	2.62	0.35	5.30	50.41	0.538
CO_2	24.62	−0.12	−1.89	2.13	−0.43	3.18	27.80	0.400
Cyanamide	75.51	2.77	−5.11	6.60	−1.28	3.65	79.16	0.095
Cytosine	163.44	−0.24	−3.14	3.43	0.54	5.37	168.81	0.294
Ethylcarbamate	78.71	−0.30	−2.29	2.49	0.50	5.46	84.17	0.331
Formamide	71.77	−1.37	−4.20	4.99	2.16	6.97	78.74	0.137
Imidazole	81.37	0.94	−3.12	3.49	−0.58	4.38	85.75	0.267
Naphthalene	71.27	0.06	−1.95	2.09	0.09	5.04	76.32	0.215
Oxalic acid (α)	93.70	3.04	−3.55	3.96	−2.63	2.32	96.02	0.496
Oxalic acid (β)	93.63	2.99	−2.62	2.87	−2.74	2.22	95.85	0.510
Pyrazine	56.27	−0.72	−2.34	2.54	0.93	5.89	62.16	0.252
Pyrazole	72.36	0.82	−3.17	3.55	−0.44	4.47	76.83	0.316
Triazine	55.66	0.21	−2.12	2.32	−0.01	4.85	60.51	0.531
Trioxane	56.25	−1.22	−1.82	1.95	1.34	6.29	62.54	0.661
Uracil	129.18	0.85	−3.05	3.27	−0.64	3.72	132.90	0.398
Urea	93.79	−0.02	−3.34	3.75	0.43	5.64	99.43	0.613

are required in order to properly carry out the benchmark calculations.

We have used the projector-augmented wave (PAW) method[66] in the plane-wave basis set scheme. The pseudopotentials were adapted from the atompaw library[67] and are the same as in our previous work,[30] but adapted to the appropriate functionals. The plane-wave kinetic energy cutoff is 80 Ry which ensures the convergence of crystal and molecular energies to around 0.1 mRy, enough to obtain accurate energy differences on the order of 0.01–0.1 kJ/mol.

In the following, the calculation of two quantities are described: sublimation enthalpies and the equilibrium geometry under a negative pressure. Both involve geometry relaxations of molecular crystals, and the former also requires the calculation of the isolated molecules in a supercell. The $\boldsymbol{k}$-point grid used in the condensed-phase calculation and the cell length in the molecular calculation have both been converged independently with respect to the total energy and are listed in Table I of the supplementary material.[68] In the particular case of vdw-DF functionals, because of memory limitations, the maximum cell length has been capped at 35 bohr. The molecular geometries and geometries were obtained from gas-phase calculations using the PBE functional[69,70] and the 6-31++G** basis set, as implemented in the GAUSSIAN09 program.[71]

IV. REFERENCE DATA

The C21 set consists of 21 crystals (see Table I of the supplementary material[68]). Four criteria have been used in the selection of these: (i) the crystals need to be small (few atoms per cell) in order to compute their vibrational properties, required for the thermal correction, in a reasonable amount of time, (ii) the sublimation enthalpies need to be known with reasonable precision, which means that there must be abundant and recent data, including the temperature range of the measurement, (iii) the crystals should not present polymorphism at room temperature and zero-pressure (except for oxalic acid, where sublimation enthalpies for both forms are available), and (iv) there must not be configurational disorder as in, for instance, the phases of ice. The chosen crystals also try to span several types of intermolecular interactions (π-stacking, electrostatic, hydrogen-bond,. . .) and interaction energies (from around 20 kJ/mol to 160 kJ/mol, see Table I below). In the following, all sublimation enthalpies and lattice energies are reported per molecule.

The C21 benchmark is based on the first-principles determination of two different properties: lattice energies, related to experimental sublimation enthalpies, and crystal structures. The former requires the calculation of the lattice energy of the molecular crystal, which is the energy required to pull the molecules apart from each other. The latter requires a geometry optimization in order to compare to x-ray diffraction data. Neither of the two can be compared directly to experimental sublimation enthalpies or crystal structures because of the effect temperature has on those quantities (mainly via atomic vibrations). Experimental data, particularly sublimation enthalpies, is subject to uncertainties which set the error bar of the benchmark. For instance, Chickos cites for the sublimation enthalpy an average experimental error of 4.9 kJ/mol,[72] so two methods that deviate on average from the reference data by an amount below this number, have both hit the precision limit of the benchmark and no assessment can

be made about their relative accuracy. On the other hand, x-ray diffraction data are accurate enough so that no method reaches the precision limit, except for the positions of the hydrogens, which we refrain from using as reference. The second source of error comes from the reduction of temperature effects on the experimental data. Because calculation of the complete vibrational profiles for these molecular crystals is unfeasible, we have to turn to reasonable but necessarily approximate estimations. As we show below, the XDM method is accurate enough to reach the precision limit of the sublimation enthalpy benchmark, while four of the explored methods are able to predict experimental cell lengths (which are controlled by non-covalent interactions in molecular crystals) with an error of 1%–2% on average, confirming *a posteriori* the soundness of our thermal corrections.

The use of sublimation enthalpies of molecular crystals to compare the behavior of different dispersion-corrected density functionals has been tried before,[22,35] but a rigorous treatment of the solid vibrations is still required. A further advantage of this treatment is that we can assess the accuracy of typical approximate corrections on the sublimation enthalpy. We point out that a usual pragmatic concession in intermolecular force field fitting is to include thermal effects by parametrizing using the experimental sublimation enthalpies in the training sets,[5] thereby including temperature effects in the static picture. In that case, direct comparison to experiment is permissible, while in the case of DFT lattice energies failing to include the thermal correction introduces a systematic bias in the analysis.

At a given temperature T, the sublimation enthalpy is

$$\Delta H_{\text{sub}} = E^g_{\text{el}} + E^g_{\text{trans}} + E^g_{\text{rot}} + E^g_{\text{vib}} + pV - \left(E^s_{\text{el}} + E^s_{\text{vib}}\right), \tag{13}$$

where g denotes gas-phase and s solid-phase quantities. The subscripts correspond to the electronic (el), translational (trans), rotational (rot), and vibrational (vib) contributions to the enthalpy. No low-lying electronic states or configurational disorder are present in our crystals. A very reasonable approximation, especially considering the low vapor pressure of molecular crystals[6] is to assume the gas is ideal, which means $E^g_{\text{trans}} = 3/2RT$, $E^g_{\text{rot}} = 3/2RT$ (or RT if the molecule is linear), and $pV = RT$. The above equation reduces to (we consider only the nonlinear molecule case for clarity)

$$\Delta H_{\text{sub}}(T) = \Delta E_{\text{el}} + \Delta E_{\text{vib}} + 4RT, \tag{14}$$

where ΔE_{el} is the (temperature-independent) difference in electronic energies calculated directly from DFT, the lattice energy. ΔE_{vib} is the difference in vibrational energies between the molecules in the gas-phase and in the solid. The intramolecular vibrational frequencies and modes in both cases are expected to be very similar, and in the case of the stiffest of those, also decoupled from intermolecular modes in the crystal. As a consequence, the vibrational contribution can be written as

$$\begin{aligned}\Delta E_{\text{vib}} &= E^g_{\text{vib}} - E^s_{\text{vib}} \\ &= E^g_{\text{vib}} - E^{s,\text{intra}}_{\text{vib}} - E^{s,\text{inter}}_{\text{vib}} \\ &= \Delta E^{\text{relax}}_{\text{vib}} - E^{s,\text{inter}}_{\text{vib}},\end{aligned} \tag{15}$$

where inter and intra denote the intermolecular and intramolecular contribution to the vibrational energy of the solid, respectively. We call $\Delta E^{\text{relax}}_{\text{vib}}$ the relaxation energy, related to the change in the frequency of the intramolecular modes when molecules pack to form the crystal. In the harmonic approximation, the internal vibrational energy is given, both in the crystal and the molecule, as[73,74]

$$E_{\text{vib}} = N_A \sum_i \frac{\omega_i}{2} + \frac{\omega_i}{e^{\omega_i/k_BT} - 1}, \tag{16}$$

where the frequencies are given in atomic units of energy, k_B is the Boltzmann constant, and N_A is Avogadro's number. In the isolated molecule, the sum goes over the $3n - 6$ vibrational modes, with n the number of atoms. In the crystal, the sum involves a weighted sampling of the first Brillouin zone (1BZ) and is usually replaced by the corresponding integral using the phonon density of states, $g(\omega)$. The density of states is normalized to $3nZ$, where Z is the number of molecules per primitive cell.

The computation of the molecular vibrational frequencies is relatively inexpensive and straightforward. The determination of $g(\omega)$, however, is complex because it involves the calculation of frequencies on a grid sampling the 1BZ. These calculations in solids have experienced great advances in recent years with the development of linear-response methods,[75,76] but for the case at hand it is still too onerous, especially given the very high-quality energy cutoff and $\boldsymbol{k}$-point sampling we need to use to reach the desired accuracy.

Fortunately, because intramolecular vibrations in molecular crystals are so stiff, they are essentially incapable of carrying energy along the crystal and the dispersion relations are virtually $\boldsymbol{q}$-independent. This is clearly shown for CO_2 in Figure 1. Therefore, a sound approximation to $g(\omega)$ is the Einstein model, in which each branch is represented by a single frequency calculated at the Γ point. For the three acoustic branches, the zero-point term is neglected and the thermal part is computed at the high temperature limit (k_BT per branch). In the particular case of CO_2 shown above, numerical integration of $g(\omega)$ gives a vibrational energy per molecule of 43.63 kJ/mol, of which 10.86 is thermal and 32.77 is

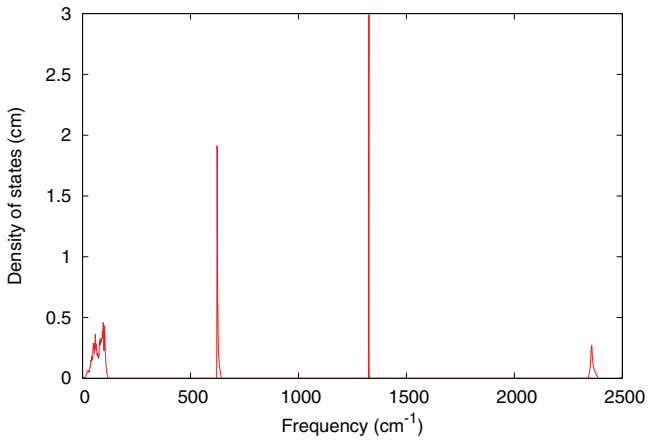

FIG. 1. The phonon density of states of CO_2, calculated at the PBE-XDM equilibrium geometry using a $4 \times 4 \times 4$ sampling grid, Fourier-reinterpolated to 50^3.

zero-point. The total energy using the Einstein model is 42.89 kJ/mol, of which 11.21 is thermal and 31.68 is zero-point. The approximation to both terms is excellent and, moreover, the larger the molecule forming the crystal is, the greater the number of intramolecular low-dispersion modes will exist. Thus, CO_2 is in this respect a worst-case scenario for the Einstein model, while the error it introduces is already negligible compared with the precision of the experimental sublimation enthalpies.

Armed with these results, the vibrational energy difference in Eq. (14) can be calculated by substracting the vibrational energy of the solid from the gas-phase molecule. The former is obtained using Eq. (16), where the frequencies at Γ are calculated using the density-functional perturbation theory[76] (DFPT) at the PBE-XDM equilibrium geometry. The vibrational energy of the gas is obtained by relaxing the geometry of the isolated molecule and calculating the frequencies at the PBE/6-31++G** level. It is important to use the same functional for both calculations to benefit from the error cancellation of the systematic deviation of the functional. To gauge the error introduced by comparing plane-wave/pseudopotentials (PWPS) to gaussian-basis-set/all-electron results, we calculated the frequencies of the CO_2 molecule in a supercell in the PWPS approach. The difference in each individual frequency is on the order of 10 cm^{-1}, which introduces a negligible difference in the vibrational energy. Table I shows the average experimental sublimation enthalpies corrected to room temperature ($\Delta H_{sub}(T^0)$, $T^0 = 298.15$ K) and the proposed corrected lattice energies (ΔE_{el}^{exp}). The latter can be used to benchmark any dispersion method by direct comparison with DFT lattice energies.

A widely used way to remove thermal effects from experimental sublimation enthalpies is to add a constant $2RT$, independent of the crystal[5,6,22,35]

$$\Delta H_{sub}(T) = \Delta E_{el} - 2RT, \tag{17}$$

where the last term would be $-3/2RT$ in the case of a linear molecule . This approximation rests on three assumptions: (i) the intramolecular frequencies are assumed to be equal in the crystal and in the gas-phase ($\Delta E_{vib}^{relax} = 0$ in Eq. (15)), (ii) the temperature is high enough to treat intermolecular vibrations as if they were at the high-temperature limit ($E_{vib}^{s,inter} = 6RT$), and (iii) the intermolecular zero-point effects can be neglected ($E_{vib,zp}^{s,inter} = 0$). Table I shows the relaxation energy, the deviation of the intermolecular vibrational energy from the high-temperature limit and the intermolecular zero-point contribution. If the $2RT$ approximation were exact, all three of them should be zero independently. While the relaxation energy is relatively small (except for both phases of oxalic acid), neither $\Delta E_{vib}^{s,inter}$ nor $E_{vib,zp}^{s,inter}$ are negligible compared to the total thermal correction or the experimental precision. Fortunately, assuming the Dulong-Petit high-temperature limit overestimates the intermolecular vibrational energy, which corrects for the missing zero-point intermolecular energy. The total deviation of the $2RT$ correction (E_{vib}^{error}) shows that this error cancellation leads, in general, to an acceptable estimate of the real value, but users should be aware that this cancellation is not valid at all temperatures (the zero-point term is temperature-independent) and that in some cases (such as ammonia or oxalic acid) the error can be significant. It is also a mistake to use the $2RT$ correction together with a zero-point correction.[26]

The comparison of equilibrium structures to diffraction data poses a different problem. In this case, the vibrations of the solid at the diffraction temperature induce a thermal expansion that introduces a systematic deviation from the static DFT equilibrium structures. The equilibrium volume V and internal coordinates $\boldsymbol{x}$ of a crystal (which include the atomic positions and cell shape) at a given temperature (T) and pressure (p) are found by minimizing the non-equilibrium Gibbs energy

$$G(\boldsymbol{x}, V; p, T) = E_{el}(\boldsymbol{x}, V) + pV + F_{vib}(\boldsymbol{x}, V; T), \tag{18}$$

where F_{vib} is the non-equilibrium vibrational Helmholtz energy. In the quasiharmonic approximation,[74] it is given by

$$F_{vib} = \sum_j \left[\frac{\omega_j}{2} + k_B T \ln(1 - e^{-\omega_j/k_B T})\right], \tag{19}$$

where frequencies depend on V and $\boldsymbol{x}$. As in the case of the vibrational energy, we use the Einstein model to reduce the computational cost of evaluating the vibrational Helmholtz energy.

Volume and $\boldsymbol{x}$ are implicit functions of T and p via minimization of G. It is a common approximation to assume that temperature effects apply primarily to volume and that the internal coordinates are determined by minimization of E_{el} constrained to a fixed volume $V(p, T)$. This *statically constrained* approximation is, in general, excellent, and also very difficult to avoid from the computational point of view.[77] Minimizing G (Eq. (18)) with respect to volume at zero pressure and constant temperature gives

$$p_{sta}(V) = -p_{th}(V, T), \tag{20}$$

where the static pressure is $p_{sta} = -dE_{el}/dV$ and the thermal pressure is $p_{th} = -dF_{vib}/dV$. The calculation of the latter involves the volume derivative of the frequencies (the Grüneisen mode γ_is) for which there is no simple estimate in molecular crystals.[78] As a consequence, the thermal pressure needs to be calculated by explicit differentiation of F_{vib} for several volumes.

To avoid sampling an extensive volume range, a further simplifying approximation can be made thanks to p_{th} depending very slightly on volume.[79] We can substitute the thermal pressure in Eq. (20) by its value at the equilibrium geometry. In practice, this means that we can approximately incorporate thermal effects into the DFT geometries by relaxing the crystal structure at a negative external pressure equal to $-p_{th}$. We compute the thermal pressure by sampling three volume points: the equilibrium geometry, and volumes reduced by 10% and 20% (the calculation is faster in compression than in expansion), and using a finite-difference formula on the calculated F_{vib}. The procedure is illustrated in Figure 2 for CO_2. The vibrational Helmholtz energy is almost linear with volume and the thermal pressure calculated from finite differences is 0.397 GPa, in excellent agreement with the value for the quartic fit to the whole curve, 0.403 GPa. The convergence criterion on the target pressure used in our DFT calculations is

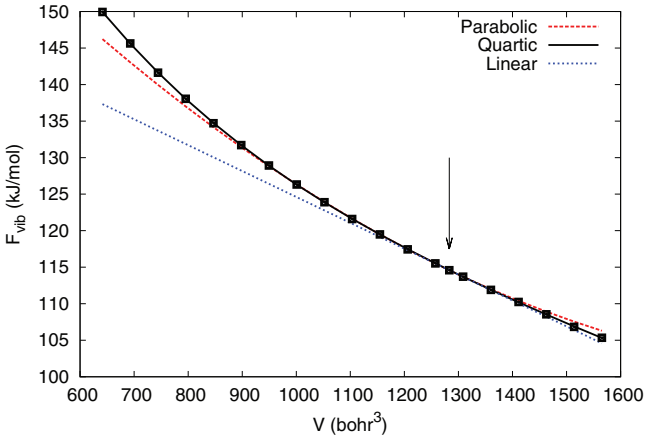

FIG. 2. The vibrational Helmholtz energy of carbon dioxide against volume is shown, together with a quartic fit (black, full line), a parabolic fit to the equilibrium volume and two points on compression (red, stippled line), and the line tangent to the vibrational energy curve at the equilibrium volume (blue, dotted line). The arrow marks the equilibrium geometry.

0.01 GPa, larger than the error in the finite-difference approximation to the derivative and five times less than the default value in Quantum ESPRESSO. A deviation of this magnitude in the pressure has a negligible impact on the geometries. The calculated thermal pressures for all crystals in the C21 set at their respective diffraction temperatures are shown in Table I.

In summary, the last two columns of Table I allow the benchmark of dispersion-corrected methods for lattice energies and geometries of molecular solids. The DFT lattice energy is directly compared to $\Delta E_{\mathrm{el}}^{\mathrm{exp}}$. By relaxing the structure at the external pressure $-p_{\mathrm{th}}$, thermal and zero-point effects on the crystal geometry are introduced and it is possible to compare to directly to experimental diffraction results.

V. BENCHMARK RESULTS

Table II and Figure 3 show the lattice energies of the C21 crystals calculated using the different functionals and compared to the reference values. The best statistics are obtained with the XDM method, especially when coupled with the B86b functional. Its accuracy (6.23%) approximately doubles that of PBE-D (11.94%) and the vdw-DF non-local functionals (10.11% and 10.22%) and is almost four times better than PBE-TS (22.08%). The PBE-XDM result is slightly worse (6.74%), which as shown before,[30] is a consequence of the spurious binding of the exchange functional. It should be noted that the mean absolute errors (MAE) for B86b-XDM (4.8 kJ/mol) is below the average experimental error proposed by Chickos[72] for sublimation enthalpy measurements (4.9 kJ/mol), so the agreement of B86b-XDM with the exact lattice energy may be even better than that value. The rest of the functionals, including PBE-XDM, however, fail to hit the precision limit of the benchmark and can be safely ranked using our reference data. By these results, B86b-XDM is shown to be a very accurate method to include dispersion interactions at a semilocal DFT computational cost. Also, all methods improve greatly the uncorrected PBE result, which grossly underestimates sublimation enthalpies, particularly

TABLE II. Lattice energies of the C21 crystals compared to the experimental reference data. The mean absolute errors (MAE) and mean absolute relative errors (MA%E) are indicated. The last two lines show the MA%E when no thermal correction and the 2*RT* term are used. Units are kJ/mol.

Name	B86b-XDM	PBE	PBE-D	PBE-TS	PBE-XDM	vdw-DF1	vdw-DF2	$\Delta E_{\mathrm{el}}^{\mathrm{exp}}$
14-cyclohexanedione	85.81	37.56	97.32	107.22	84.64	104.39	103.33	86.53
Acetic acid	71.76	48.12	77.60	83.66	72.52	77.38	78.10	71.80
Adamantane	72.80	−0.35	83.94	108.92	69.83	82.56	79.48	62.43
Ammonia	38.56	28.86	46.23	44.03	39.15	37.47	40.31	37.57
Anthracene	101.23	14.77	106.22	135.46	96.29	116.98	108.55	100.58
Benzene	51.23	10.57	56.32	66.51	49.49	59.94	55.87	50.41
CO_2	21.55	10.46	24.37	25.72	22.63	35.76	33.81	27.80
Cyanamide	87.24	67.51	92.43	94.10	87.75	84.58	88.40	79.16
Cytosine	151.25	104.24	163.83	172.82	150.25	153.92	157.53	168.81
Ethylcarbamate	83.76	50.83	92.82	99.49	84.18	95.96	95.92	84.17
Formamide	77.95	59.63	84.12	86.79	78.65	79.22	82.56	78.74
Imidazole	87.54	57.09	94.46	100.76	87.32	89.99	89.58	85.75
Naphthalene	75.74	11.35	80.40	100.53	72.24	88.06	81.44	76.32
Oxalic acid (α)	111.28	81.05	119.65	125.17	112.12	120.25	125.43	96.02
Oxalic acid (β)	113.81	85.45	122.95	128.20	114.99	120.77	124.70	95.85
Pyrazine	59.66	21.83	64.47	74.90	58.48	69.09	67.75	62.16
Pyrazole	75.99	46.78	83.65	87.69	75.76	79.40	79.18	76.83
Triazine	54.73	20.30	61.20	67.98	53.93	68.38	66.50	60.51
Trioxane	57.95	23.37	67.23	75.78	57.34	77.64	79.31	62.54
Uracil	130.42	87.27	138.21	150.21	130.19	137.31	140.01	132.90
Urea	101.91	77.23	112.02	112.62	102.51	101.93	108.28	99.43
MAE	4.81	35.83	9.05	16.97	5.35	10.22	10.11	
MA%E	6.23	47.22	11.94	22.08	6.74	13.53	13.11	
MA%E (no correction)	10.10	43.32	18.99	30.47	9.40	21.75	21.35	
MA%E (plus 2*RT*)	6.42	47.23	12.27	22.37	6.98	13.15	12.80	

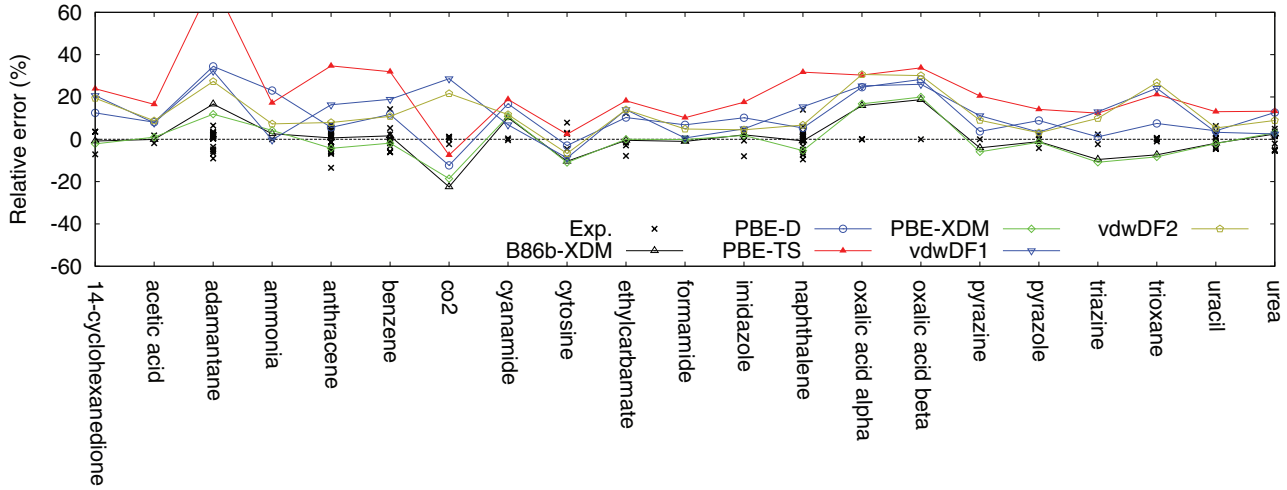

FIG. 3. Graphical representation of the lattice energy errors relative to the reference value for all the functionals used. The black crosses mark single experimental results and give an idea of the spread and quality of the reference.

for dispersion-bound crystals, such as benzene, naphthalene, anthracene, or adamantane.

Next to XDM, PBE-D, and the vdw-DF functionals achieve a MAE around 10 kJ/mol, with PBE-D giving slightly better results. Because the crystal selection is restricted to organic molecules, the C21 set is favorable for PBE-D. Future work will explore surface adsorption and lattice energies of organometallic crystals (for instance, ferrocene, for which extensive sublimation enthalpy data are available). The newer vdw-DF2 does not seem to improve appreciably the energetics with respect to vdw-DF1. Lastly, PBE-TS results are rather poor (MAE 16.97 kJ/mol), which is curious especially considering the good performance for the S22 set.[32] Our results for CO_2, benzene, naphthalene, anthracene, and cytosine are consistent with Ref. 31, and the geometries predicted by PBE-TS are good (see below), which at first sight rules out errors in the implementation. Certainly, the problem of weak interactions in molecular solids, where many different types of noncovalent bonding situations happen concurrently is different (and possibly tougher, as the statistics show) than dimer binding. This result warns against judging performance from the S22 statistics alone when shifting from molecules to solids, particularly if this database has been used as a training set for the functional.

The vdw-DF functionals, PBE-D, and especially PBE-TS, are clearly biased towards overbinding. A possible explanation of this effect in the case of PBE-D and PBE-TS comes from the higher order pairwise contributions to the dispersion energy. Contrary to XDM, both methods only include the leading R^{-6} term in the dispersion expansion, and use a combination of overestimated C_6 coefficients derived from the free-atom values and the damping function to account for the missing stabilizing energy. For instance, the $C_{6,ii}$ for carbon in benzene (atomic units) are 19.72 (B86b-XDM), 19.56 (PBE-XDM), 32.27 (PBE-TS), and 30.35 (PBE-D). The PBE-TS and PBE-D coefficients are more than 60% larger than their XDM equivalents, a trend that is repeated for other crystals and atoms. The damping parameters are fit to a training set of dimers, which are much less densely packed than molecular crystals. Intermolecular interactions in the solid, that should be decaying like R^{-8} and R^{-10}, are represented by a R^{-6} term and, because their number is much greater than in the training set, the dispersion energy is overestimated. The success of XDM can, therefore, be explained by the introduction of higher order terms and the lack of reference to the free-atom interaction coefficients, which are much larger than the in-molecule ones.[58] The overestimation of the lattice energies by vdw-DF functionals is, however, not explained by this hypothesis.

Another possible explanation for the overestimation is the lack of the non-additive many-body effects in the dispersion energy expansion. The leading three-body term (corresponding to a triple-dipole interaction, the Axilrod-Teller-Muto term) is, in general, repulsive in condensed phases and could lead to a correction to PBE-TS and PBE-D systematic deviations. In a recent article, Tkatchenko *et al.*[80] report that including the non-additive many-body contributions to the dispersion energy reduces the overestimation in PBE-TS and improves its S22 statistics, in line with previous observations of the relative importance of this term.[81] The evaluation of the many-body contributions (particularly the triple-dipole Axilrod-Teller-Muto term) in XDM is possible and will be the subject of a future work.

It has been argued before[35] that the $2RT$ correction to the sublimation enthalpy should not be included when comparing static lattice energies to sublimation enthalpies. Table II shows that this is clearly not the case. Using the uncorrected sublimation enthalpies doubles the MAE because the reference is shifted to smaller values, increasing the overbinding. The $2RT$ correction gives MAE similar to, but slightly larger than, those obtained using the rigorous thermal correction, except in the case of vdw-DF.

Table III and Table 2 of the supplementary material[68] compare the equilibrium geometries at $-p_{\text{th}}$ external pressure with diffraction data. The agreement of B86b-XDM, PBE-D, vdw-DF2, and PBE-TS with experiment is remarkable, predicting cell lengths within 1%–2% (a little more than 0.1 bohr) of the correct result, angles within 0.2%, and errors in

TABLE III. Mean absolute and relative deviations of cell lengths, angles, and atomic positions. The coordinates of hydrogen atoms have not been included in the statistics. Length units are bohr.

Name	B86b-XDM	PBE-D	PBE-TS	PBE-XDM	vdw-DF1	vdw-DF2
MAD lengths	0.12	0.11	0.10	0.20	0.31	0.14
MA%D lengths	1.76	1.31	1.58	2.75	4.40	1.88
MAD angles	0.17	0.19	0.14	0.29	0.11	0.13
MA%D angles	0.16	0.18	0.13	0.27	0.10	0.12
MAD internal	0.00063	0.00046	0.00054	0.00085	0.00050	0.00032

the internal coordinates in the order of 10^{-3}–10^{-4}. The latter value indicates that intramolecular interactions involving covalent bonds are not affected by the dispersion correction and the excellent GGA description of covalent distances prevails. Curiously, in spite of its poor statistics for energetics, PBE-TS cell lengths are accurate. It is clear from these results that good agreement with experimental geometries does not automatically ensure good energetics.

PBE-D, B86b-XDM, and vdw-DF2 are in the same accuracy range, with lengths predicted better in that order and angles in the reverse order. PBE-XDM gives poorer results than B86b-XDM, even more so than in the case of lattice energies, with a MA%D escalating up to 2.75%. The PBE-XDM cell lengths are on average 0.20 bohr away from the experimental values, which we still consider usable. Also, there is a great improvement in vdw-DF2 compared to vdw-DF1, correcting the systematic overestimation of the cell lengths, in agreement with previous results.[29,33]

VI. CONCLUSIONS

In this article, we propose the C21 set, a benchmark for non-covalent interactions in molecular solids based on experimental sublimation enthalpies and diffraction crystal geometries. Using a careful procedure involving reasonable physical and numerical approximations, we take into account thermal and zero-point effects on both measures. Sublimation enthalpies are reduced to lattice energies, directly comparable to electronic-structure static results. Diffraction data can be compared with static results by optimizing the crystal structure under an external pressure equal to the thermal pressure, which is calculated from the vibrations of the crystal. We used the new benchmark to assess the performance of several dispersion-corrected functionals: DFT-D2 (PBE), Tkatchenko-Scheffler (PBE-TS), two non-local functionals by Langreth *et al.* (vdw-DF1 and vdw-DF2), and the XDM model, recently implemented in solids (B86b-XDM and PBE-XDM). The most accurate results are obtained with B86b-XDM, which predicts lattice energies with a mean absolute deviation of 4.8 kJ/mol, less than the experimental precision for sublimation enthalpy measurements (4.9 kJ/mol). Also, lattice constants are in agreement with experiment within 1%–2%, cell angles within 0.1%–0.2% and the deviation in the atomic coordinates is in the range of 10^{-4}–10^{-3}.

B86b-XDM is confirmed as an excellent method for lattice energies and geometries of molecular crystals and further applications to surface adsorption and polymorph ranking are in progress. The lattice energies are predicted with a mean absolute percent error (6.23%) that at least roughly doubles the accuracy of other common approaches in the literature (PBE-D, PBE-TS, vdw-DF1, vdw-DF2), while still offering very good crystal geometries and retaining the computational cost of a semilocal DFT calculation. In contrast, PBE-XDM presents poorer energetics and geometries than B86b-XDM because of the spurious binding of the exchange functional. While the crystal structures predicted by PBE-D and PBE-TS are in very good agreement with diffraction data, their lattice energies are affected by overbinding, possibly caused by neglecting the higher order terms in the dispersion asymptotic formula. The most recent non-local functional, vdw-DF2, does not predict better lattice energies but greatly improves the crystal geometries compared to vdw-DF1.

ACKNOWLEDGMENTS

A.O.R. thanks the Spanish Malta/Consolider initiative (No. CSD2007-00045).

[1] E. R. Johnson, I. D. Mackie, and G. A. DiLabio, J. Phys. Org. Chem. **22**, 1127 (2009).
[2] A. Tkatchenko, L. Romaner, O. T. Hofmann, E. Zojer, C. Ambrosch-Draxl, and M. Scheffler, MRS Bull. **35**, 435 (2010).
[3] S. Grimme, Comput. Mol. Sci. **1**, 211 (2011).
[4] J. F. Dobson and T. Gould, J. Phys.: Condens. Matter **24**, 073201 (2012).
[5] A. Gavezzotti, *Theoretical Aspects and Computer Modeling of the Molecular Solid State* (Recherche, 1997), Vol. 67.
[6] A. Gavezzotti, *Molecular Aggregation: Structure Analysis and Molecular Simulation of Crystals and Liquids* (Oxford University Press, New York, 2007), Vol. 19.
[7] M. A. Neumann, F. J. J. Leusen, and J. Kendrick, Angew. Chem. Int. Ed. **47**, 2427 (2008).
[8] G. R. Desiraju, Angew. Chem. Int. Ed. **46**, 8342 (2007).
[9] A. J. Cohen, P. Mori-Snchez, and W. Yang, Chem. Rev. **112**, 289 (2012).
[10] J. Tao, J. P. Perdew, and A. Ruzsinszky, Proc. Natl. Acad. Sci. U.S.A. **109**, 18 (2012).
[11] K. T. Tang and J. P. Toennies, J. Chem. Phys. **118**, 4976 (2003).
[12] P. Jurečka, J. Šponer, J. Černý, and P. Hobza, Phys. Chem. Chem. Phys. **8**, 1985 (2006).
[13] E. R. Johnson and A. D. Becke, J. Chem. Phys. **124**, 174104 (2006).
[14] F. O. Kannemann and A. D. Becke, J. Chem. Theory Comput. **6**, 1081 (2010).
[15] L. Grafova, M. Pitonak, J. Rezac, and P. Hobza, J. Chem. Theory Comput. **6**, 2365 (2010).
[16] J. Rezac, K. E. Riley, and P. Hobza, J. Chem. Theory Comput. **7**, 2427 (2011).
[17] F. Ortmann, F. Bechstedt, and W. G. Schmidt, Phys. Rev. B **73**, 205101 (2006).
[18] S. Feng and T. Li, J. Chem. Theory Comput. **2**, 149 (2006).
[19] A. L. Ringer and C. D. Sherrill, Chem. Eur. J. **14**, 2542 (2008).
[20] R. Podeszwa, B. M. Rice, and K. Szalewicz, Phys. Rev. Lett. **101**, 115503 (2008).

[21]O. Bludský, M. Rubes, and P. Soldán, Phys. Rev. B **77**, 092103 (2008).
[22]B. Civalleri, C. M. Zicovich-Wilson, L. Valenzano, and P. Ugliengo, Cryst. Eng. Comm. **10**, 405 (2008).
[23]V. Barone, M. Casarin, D. Forrer, M. Pavone, M. Sambi, and A. Vittadini, J. Comput. Chem. **30**, 934 (2009).
[24]D. Lu, Y. Li, D. Rocca, and G. Galli, Phys. Rev. Lett. **102**, 206411 (2009).
[25]Y. Li, D. Lu, H.-V. Nguyen, and G. Galli, J. Phys. Chem. A **114**, 1944 (2010).
[26]G. J. O. Beran and K. Nanda, J. Phys. Chem. Lett. **1**, 3480 (2010).
[27]T. Bucko, J. Hafner, S. Lebegue, and J. G. Angyan, J. Phys. Chem. A **114**, 11814 (2010).
[28]N. Marom, A. Tkatchenko, M. Rossi, V. V. Gobre, O. Hod, M. Scheffler, and L. Kronik, J. Chem. Theory Comput. **7**, 3944 (2011).
[29]K. Berland, Ø. Borck, and P. Hyldgaard, Comput. Phys. Commun. **182**, 1800 (2011).
[30]A. Otero-de-la Roza and E. R. Johnson, J. Chem. Phys. **136**, 174109 (2012).
[31]W. A. Al-Saidi, V. K. Voora, and K. D. Jordan, J. Chem. Theor. Comput. **8**, 1503 (2012).
[32]A. Tkatchenko and M. Scheffler, Phys. Rev. Lett. **102**, 073005 (2009).
[33]K. Lee, E. D. Murray, L. Kong, B. I. Lundqvist, and D. C. Langreth, Phys. Rev. B **82**, 081101 (2010).
[34]A. L. Ringer, "From small to big: understanding noncovalent interactions in chemical systems from quantum mechanical models," Ph.D. dissertation (School of Chemistry and Biochemistry, Georgia Institute of Technology, Atlanta, GA, 2009).
[35]L. Maschio, B. Civalleri, P. Ugliengo, and A. Gavezzotti, J. Phys. Chem. A **115**, 11179 (2011).
[36]J. Klimes, D. R. Bowler, and A. Michaelides, Phys. Rev. B **83**, 195131 (2011).
[37]W. Acree, Jr. and J. S. Chickos, J. Phys. Chem. Ref. Data **39**, 043101 (2010).
[38]E. R. Johnson and A. D. Becke, J. Chem. Phys. **123**, 024101 (2005).
[39]A. D. Becke and E. R. Johnson, J. Chem. Phys. **122**, 154104 (2005).
[40]A. D. Becke and E. R. Johnson, J. Chem. Phys. **123**, 154101 (2005).
[41]A. D. Becke and E. R. Johnson, J. Chem. Phys. **124**, 014104 (2006).
[42]E. R. Johnson and A. D. Becke, Chem. Phys. Lett. **432**, 600 (2006).
[43]A. D. Becke and E. R. Johnson, J. Chem. Phys. **127**, 124108 (2007).
[44]A. D. Becke and E. R. Johnson, J. Chem. Phys. **127**, 154108 (2007).
[45]F. O. Kannemann and A. D. Becke, J. Chem. Theory Comput. **5**, 719 (2009).
[46]A. D. Becke, A. Arabi, and F. O. Kannemann, Can. J. Chem. **88**, 1057 (2010).
[47]S. Grimme, J. Comput. Chem. **27**, 1787 (2006).
[48]M. Dion, H. Rydberg, E. Schröder, D. C. Langreth, and B. I. Lundqvist, Phys. Rev. Lett. **92**, 246401 (2004).
[49]F. L. Hirshfeld, Theor. Chim. Acta **44**, 129 (1977).
[50]F. O. Kannemann and A. D. Becke, J. Chem. Phys. **136**, 34109 (2012).
[51]A. D. Becke and M. R. Roussel, Phys. Rev. A **39**, 3761 (1989).
[52]J. Kong, Z. Gan, E. Proynov, M. Freindorf, and T. R. Furlani, Phys. Rev. A **79**, 042510 (2009).
[53]D. J. Lacks and R. G. Gordon, Phys. Rev. A **47**, 4681 (1993).
[54]A. D. Becke, J. Chem. Phys. **85**, 7184 (1986).
[55]J. P. Perdew and Y. Wang, Phys. Rev. B **33**, 8800 (1986).
[56]J. P. Perdew, K. Burke, and M. Ernzerhof, Phys. Rev. Lett. **77**, 3865 (1996).
[57]S. Grimme, J. Comput. Chem. **25**, 1463 (2004).
[58]E. R. Johnson, J. Chem. Phys. **135**, 234109 (2011).
[59]J.-D. Chai and M. Head-Gordon, Phys. Chem. Chem. Phys. **10**, 6615 (2008).
[60]S. Grimme, J. Antony, S. Ehrlich, and H. Krieg, J. Chem. Phys. **132**, 154104 (2010).
[61]T. Thonhauser, V. R. Cooper, S. Li, A. Puzder, P. Hyldgaard, and D. C. Langreth, Phys. Rev. B **76**, 125112 (2007).
[62]Y. Andersson, D. C. Langreth, and B. I. Lundqvist, Phys. Rev. Lett. **76**, 102 (1996).
[63]G. Román-Pérez and J. M. Soler, Phys. Rev. Lett. **103**, 096102 (2009).
[64]Y. Zhang and W. Yang, Phys. Rev. Lett. **80**, 890 (1998).
[65]P. Giannozzi, S. Baroni, N. Bonini, M. Calandra, R. Car, C. Cavazzoni, D. Ceresoli, G. L. Chiarotti, M. Cococcioni, and I. Dabo *et al.*, J. Phys.: Condens. Matter **21**, 395502 (2009).
[66]P. E. Blöchl, Phys. Rev. B **50**, 17953 (1994).
[67]N. A. W. Holzwarth, A. R. Tackett, and G. E. Matthews, Comput. Phys. Commun. **135**, 329 (2001).
[68]See supplementary material at http://dx.doi.org/10.1063/1.4738961 for minor details on the crystals (Table 1), results of geometry optimizations (Table 2), and the C21 database files.
[69]A. D. Becke, J. Chem. Phys. **98**, 5648 (1993).
[70]C. Lee, W. Yang, and R. G. Parr, Phys. Rev. B **37**, 785 (1988).
[71]M. J. Frisch, G. W. Trucks, H. B. Schlegel *et al.*, GAUSSIAN 09 Revision A.1, Gaussian Inc. Wallingford, CT, 2009.
[72]J. S. Chickos, Netsu Sokutei **30**, 116 (2003).
[73]D. A. McQuarrie and J. D. Simon, *Molecular Thermodynamics* (University of Science Books, Sausalito, CA, 1999).
[74]A. Otero-de La-Roza, D. Abbasi-Pérez, and V. Luaña, Comput. Phys. Commun. **182**, 2232 (2011).
[75]S. Baroni, P. Giannozzi, and A. Testa, Phys. Rev. Lett. **58**, 1861 (1987).
[76]S. Baroni, S. de Gironcoli, A. Dal Corso, and P. Giannozzi, Rev. Mod. Phys. **73**, 515 (2001).
[77]P. Carrier, J. F. Justo, and R. M. Wentzcovitch, Phys. Rev. B **78**, 144302 (2008).
[78]R. Zallen, Phys. Rev. B **9**, 4485 (1974).
[79]O. L. Anderson, J. Phys. Chem. Solids **58**, 335 (1997).
[80]A. Tkatchenko, R. A. DiStasio, R. Car, and M. Scheffler, Phys. Rev. Lett. **108**, 236402 (2012).
[81]O. A. von Lilienfeld and A. Tkatchenko, J. Chem. Phys. **132**, 234109 (2010).